Available online at www.sciencedirect.com
SCIENCE DIRECT
Catalysis Today 107–108 (2005) 302–309
CATALYSIS TODAY
www.elsevier.com/locate/cattod

Modifications of the citral hydrogenation selectivities over Ru/KL-zeolite catalysts induced by the metal precursors

Jesús Álvarez-Rodríguez [a,b,c], Antonio Guerrero-Ruiz [a,b], Inmaculada Rodríguez-Ramos [b,c], Adolfo Arcoya-Martín [b,c,*]

[a] *Dpto. Química Inorgánica y Técnica, UNED, Senda del Rey No. 9, 28040 Madrid, Spain*
[b] *Grupo de Diseño y Aplicación de Catalizadores Heterogéneos, Unidad Asociada UNED-ICP(CSIC), Spain*
[c] *Instituto de Catálisis y Petroleoquímica, CSIC, C/ Marie Curie No. 2, Cantoblanco, 28049 Madrid, Spain*

Available online 29 September 2005

Abstract

Three Ru/KL-zeolite catalysts containing 2 wt% of Ru were prepared from $Ru_3(CO)_{12}$, $RuNO(NO_3)_3$ and $Ru(C_5H_7O_2)_3$ precursors. The samples named Ru(c)/KL, Ru(n)/KL and Ru(a)/KL were studied by temperature-programmed reduction (TPR), by microcalorimetry of CO adsorption, by volumetric hydrogen chemisorption, by X-ray diffraction (XRD) and also by infrared spectroscopy of the CO adsorbed species (CO-FTIR). The catalytic activities and selectivities were evaluated in the hydrogenation of citral at 323 K and 5 MPa, in a stirred batch reactor. Metal dispersion follows the order Ru(c)/KL > Ru(n)/KL > Ru(a)/KL. The CO-FTIR spectra show a set of different ruthenium species on the support, suggesting the presence of large metal particle outside the zeolite and small crystallites inside the channels, the latter being majority in the Ru(c)/KL sample. Hydrogenation activity per surface metal atom (TOF) was found to be independent on the metal dispersion and, consequently, on the precursor used. The selectivity towards unsaturated alcohols (geraniol + nerol) is in the order Ru(c)/KL < Ru(a)/KL = Ru(n)/KL, while the citronellal selectivity is maximum over the Ru(c)/KL catalyst. This latter effect can be correlated to the special catalytic properties of the smaller Ru particles located inside the zeolite cavities.

Keywords: Ruthenium catalysts; Selective hydrogenation; Citral; Geraniol; Nerol; Citronellal; KL-Zeolite; CO-FTIR; Adsorption microcalorimetry

1. Introduction

The selective catalytic hydrogenation of α,β-unsaturated aldehydes to the corresponding unsaturated alcohols has attracted much interest in the recent years, because of the relevance of these compounds in the fine chemical and pharmaceutical industries. A lot of attempts have been made to develop heterogeneous catalysts suitable for these reactions. Moreover, different approaches have been used to improve the generally low selectivity of the catalysts to the desired alcohols or to other important products. It is known that the final selectivity of an active metal can be modified by employing an adequate support, which interacts with the metal, or by adding a second component, which acts as a promoter. Electronic and geometric effects have been suggested as the explanation for the improvement in selectivity towards the unsaturated alcohols.

Earlier studies carried out on hydrogenation of α,β-unsaturated aldehydes proved that unpromoted metallic catalysts have specific selectivities towards unsaturated alcohols. Iridium and osmium are rather selective; palladium, rhodium and nickel are unselective or little selective; platinum, ruthenium and cobalt are moderately selective [1]. The intrinsic selectivities of the metals have been explained in terms of the different radial expansion of their d bands [2]. Singh and Vannice [3] investigated the citral hydrogenation over SiO_2-supported groups VIII metals in the liquid-phase and found that Os, Ru and Co exhibit high selectivity towards unsaturated alcohol isomers, while Ni, Pd and Rh are highly selective to citronellal and isopulegol.

On other hand, the environment of the metal particles can produce steric constraints, which orientate the adsorption of the reactant molecules and direct the selectivity of the

* Corresponding author.
E-mail address: aarcoya@icp.csic.es (A. Arcoya-Martín).

0920-5861/$ – see front matter © 2005 Elsevier B.V. All rights reserved.
doi:10.1016/j.cattod.2005.07.088

reaction. Thus, metal clusters (Pt, Rh, Ru) located in the cages of Y and beta zeolites have been reported to be very selective catalytic systems for the production of unsaturated alcohols [4–6]. This high selectivity was attributed to molecular constraints in the zeolite microporous cages, which force the reactant molecule to adsorb on the encaged metal particles via the C=O group and hamper the adsorption of the C=C bond.

In addition, the mode of adsorption of the α,β-unsaturated aldehyde molecules can be governed by the electronic structure of the metal surface. Thus, enrichment of the metal surface with electrons by interactions with a support or ligand could, on the one hand, decrease the binding energy of the C=C bond via an increase of the repulsive four-electron interaction and, on the other hand, favor the backbonding interaction with the π^*_{CO}-orbital and the hydrogenation of the C=O bond with respect to that of C=C. Finally, when the reaction is conducted in liquid phase the nature of the solvent may have an important effect on the selectivity of the reaction. Mäki-Arvela et al. [7] studied the hydrogenation of citral in liquid phase with different solvents and they found that side reactions, acetalization and cyclization, can be diminished by using longer chained alcohols, like 2-pentanol or 2-methyl-2-propanol, as solvents.

KL is a non-acidic synthetic zeolite whose structure consists of a tri-dimensional system with a channel constituted by cages of 0.48 nm × 1.24 nm × 1.07 nm, connected by windows of 12-membered rings with a diameter of 0.71 nm [8]. Catalysts of platinum supported on KL zeolite have been reported to be highly active and selective in the dehydrocyclization of light alkanes due, in part, to the singular property of the zeolite to stabilize electron rich metallic particles inside the channels [9–11]. In order to evaluate the KL-zeolite as a support and obtain catalysts with different physicochemical properties for the selective hydrogenation of α,β-unsaturated aldehydes, we have prepared several Ru/KL samples using different ruthenium precursors. Since KL is a non-acidic zeolite [8], it is expected that reactions involving acid sites are minimized. For the same reason, we have used chloride free ruthenium precursors and 2-propanol as solvent. The catalysts were characterized by X-ray diffraction (XRD), hydrogen chemisorption, temperature-programmed reduction (TPR), infrared spectroscopy of CO chemisorbed (CO-FTIR) and microcalorimetry of CO adsorption. The catalytic behavior was studied in the hydrogenation reaction of citral to unsaturated alcohols and citronellal and the results were associated with the size of the ruthenium particles and their interaction with the support.

2. Experimental

2.1. Catalyst preparation

Three catalysts containing 2 wt% of ruthenium were prepared using a commercial KL-zeolite as support (Union Carbide, SK-45, $K_9Al_9Si_{27}O_{72}$ in atoms per unit cell and average particle grain, 53 μm) previously calcined at 873 K for 3 h. Two portions of this support were impregnated with ruthenium (III) 2,4-pentanedionate (Alpha Aesar) and tri-ruthenium dodecacarbonile (Aldrich) acetone solutions, respectively. Another catalyst was prepared from an aqueous solution of ruthenium (III) nitrosylnitrate (Alpha Aesar). After drying at 393 K overnight, all the samples were reduced at atmospheric pressure under hydrogen flow at 673 K for 2 h and then cooled down to room temperature under inert flow.

2.2. Catalysts characterization

The number of exposed metal atoms was measured by hydrogen chemisorption at 373 K using a conventional volumetric system. A catalyst sample (300 mg) previously reduced at 673 K under hydrogen atmosphere, was outgassed at the same temperature for 2 h. After cooling down at 373 K successive hydrogen pulses were introduced between 66 and 13.100 Pa and the loss of pressure due to the adsorption was measured. Measurements were conducted at 373 K, due to the characteristic activated hydrogen chemisorption on ruthenium catalysts [12]. The hydrogen uptake was determined extrapolating to zero pressure the linear portion of the adsorption isotherm. Metal dispersions of the catalysts (D_H) is defined as $D_H = 100\ Ru_S/Ru_L$ where Ru_S is the number of exposed Ru atoms per gram of catalyst and Ru_L is the total number of Ru atoms per gram of catalyst, as determined by an inductively coupled plasma-atomic emission spectrometer (ICP-AES). The number of exposed metal atoms was calculated assuming an atomic stoichiometry Ru/H = 1/1 [13].

Heats CO adsorption measurements were performed in a Tian Calvet heat-flow microcalorimeter (Setaram C-80 II) operated isothermally at 330 K and connected to a glass vacuum-dosing apparatus. The apparatus has been described in detail elsewhere [14]. The catalysts samples were first reduced in situ under hydrogen flow at 673 K for 2 h, outgassed overnight at the same temperature and cooled to 330 K. Pulses of the probe gas (12 ml) were introduced into the system to titrate the metal surface of the sample. Both calorimetric and volumetric data were stored and evaluated by microcomputer processing. In this case, metal dispersion (D_{CO}) was calculated from the total CO uptake at the monolayer (N_{CO}), considered to be attained when the evolved heat falls to the physisorption field (40 kJ/mol), and assuming a molar stoichiometry Ru/CO = 1/1 [15]. The average particle sizes were calculated from the dispersion values, assuming spherical metal particles, d (nm) = 1.32/D_{CO} [16].

Temperature-programmed reduction (TPR) experiments were carried out in dynamic, employing a U-shape quartz reactor. The TPR profiles were registered heating the samples from room temperature to 973 K at 2.5 K min^{-1} under a flow of 10% H_2/He mixture (20 ml min^{-1}). The gas effluents of the reactor were analyzed in a gas chromato-

graph, provided with an automatic injection valve, a thermal conductivity detector and a Porapack Q column.

The crystallinity of the catalysts was studied by X-ray diffraction in a Seifert C-3000 powder diffractometer using Cu Kα radiation at 40 mA and 40 kV.

FTIR spectra of CO-chemisorbed (CO-FTIR) were registered at room temperature in a Nicolet 5ZDX spectrometer with a resolution of 4 cm^{-1} and 128 scans. The self-supported wafer of the sample (15 mg cm^{-2} density and 0.1 mm of thickness) was successively outgassed at room temperature and 2×10^3 Pa for 1 h, treated at 573 K under hydrogen flow (20 ml min^{-1}) for 2 h and evacuated later at 10^{-1} Pa at the same temperature for 1 h. After cooling to room temperature, the background spectrum was recorded and then 2 kPa of Co was introduced for 5 min at room temperature and a new spectrum was recorded. The CO adsorption spectrum was obtained by subtraction of the preceding one and the number and position of the component bands were estimated by Fourier self-deconvolution (FSD) after basis line correction. More information on the nature of the superficial metal species was obtained from the CO spectra registered after outgassing at 473 K for 10 min.

2.3. Catalytic activity measurements

Catalytic activity of the samples was evaluated in the hydrogenation of citral. The reaction was performed in a stainless steel reactor of 300 ml (Autoclaves Engineers) provided with a Magne Drive II agitation system, refrigeration and furnace system, operated in a batch mode. A mixture 0.5 ml of citral (Fluka, 97%) and 100 ml of 2-propanol (Panreac, 99.7%), with 0.5 g of catalyst in suspension, was charged in the reactor and stirred at 500 rpm. After outgassing with helium flow, the temperature was raised to 323 K, hydrogen fed and pressure adjusted at 5 MPa. Hydrogen (U-N45) was previously passed through a deoxo purifier and a 5A molecular sieve filter. When the reaction conditions were reached a sample of the reacting mixture was taken and this moment was considered as the zero time of the reaction. Reaction progress with time was followed by taking liquid samples periodically from the reactor. The samples were analyzed in gas chromatograph equipped with a flame ionization detector and a MFE-20 capillary column. It has previously been verified that under the experimental conditions used both external and internal diffusional limitations were absent and the process was essentially controlled by the surface chemical reaction [17].

3. Results and discussion

3.1. Catalysts characterization

Diffraction patterns of the catalysts display the main diffraction lines of the KL zeolite at $2\theta = 5.50$, 11.77, 22.66, 28.00 and 30.70 [8] showing that the crystallinity of the support was not modified during the catalysts preparation. Lines corresponding to ruthenium crystals were not perceived in the diffraction patterns owing to the high number of reflections stemming from the zeolite.

Table 1
Nomenclature and characterization of the KL-zeolite ruthenium catalysts

Catalyst	Precursor	Ru (wt%)	D_{CO} (%)	D_H (%)	d (nm)
Ru(c)/KL	$Ru_3(CO)_{12}$	1.96	45	39	2.8
Ru(n)/KL	$RuNO(NO_3)_3$	2.03	30	25	4.5
Ru(a)/KL	$Ru(C_5H_7O_2)_3$	1.99	17	15	7.3

D_{CO}, dispersion measured by CO chemisorption; D_H, dispersion measured by H_2 chemisorption; d, average ruthenium particle size.

Table 1 summarizes Ru loading (Ru_L), metal dispersion (D_H and D_{CO}) and average particle size (d). Metal dispersion values are different for each catalyst are different and follow the trend: Ru(c)/KL > Ru(n)/KL > Ru(a)/KL, indicating that the ruthenium dispersion is strongly related to the nature of the ruthenium precursor. On other hand, the average particle sizes, within the range of those reported for other ruthenium catalysts [18,19], are larger than the dimensions of the zeolite channels (0.48 nm × 1.24 nm × 0.71 nm). This result suggests that at least part of the metal is at the outer surface of the support, i.e. in the intercrystalline spaces of the zeolite. It should be also noted that the metallic dispersion values, obtained by both CO and H_2 chemisorptions, are in good agreement and so only an average metal size is given in Table 1 (this corresponds to the CO chemisorption).

The TPR profiles in Fig. 1 show that the reduction of the catalyst precursors occurs below 600 K, indicating that under the reduction treatment employed, all catalysts were completely reduced. It was previously observed that the TPR experiment on unloaded zeolite does not show hydrogen consumption. The profile of Ru(n)/KL exhibits a peak at 495 K with a shoulder at 460 K. On the other hand, Ru(a)/KL shows two overlapped peaks with maxima at 409 and 469 K. The two hydrogen consumption peaks suggest that the reduction of the ruthenium precursors occurs in two steps. However, since the catalyst was not subjected to calcination treatment we believe that the profiles in Fig. 1 also include the reduction of the products obtained from the metal precursor decomposition, i.e. ruthenium and anionic groups. This latter was confirmed by the gas chromatographic analysis of the effluent gas. The position of the reduction peaks of Ru(n)/KL, at higher temperature compared to those of Ru(a)/KL, suggest a greater difficulty to decompose and reduce the surface nitrate species. The TPR profile of the Ru(c)/KL precursor (no included) does not show hydrogen consumption. However, a single peak of CO with the maximum at 353 K was detected, which is attributed to the decomposition of the $Ru_3(CO)_{12}$ precursor.

The CO-FTIR spectra of the three catalysts depicted in Fig. 2 are very similar. They display a weak band at ca. 2132 cm^{-1} (HF_1) and an asymmetric broad band between

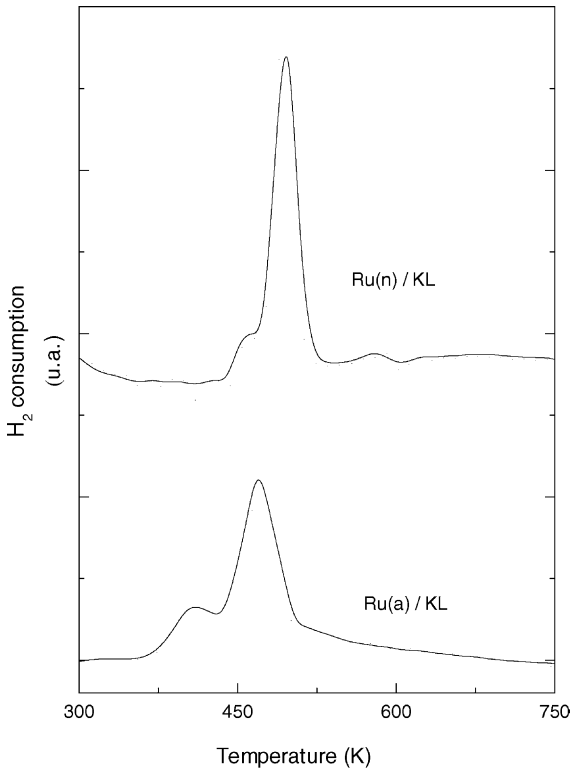

Fig. 1. TPR profiles of the catalysts Ru(n)/KL and Ru(a)/KL.

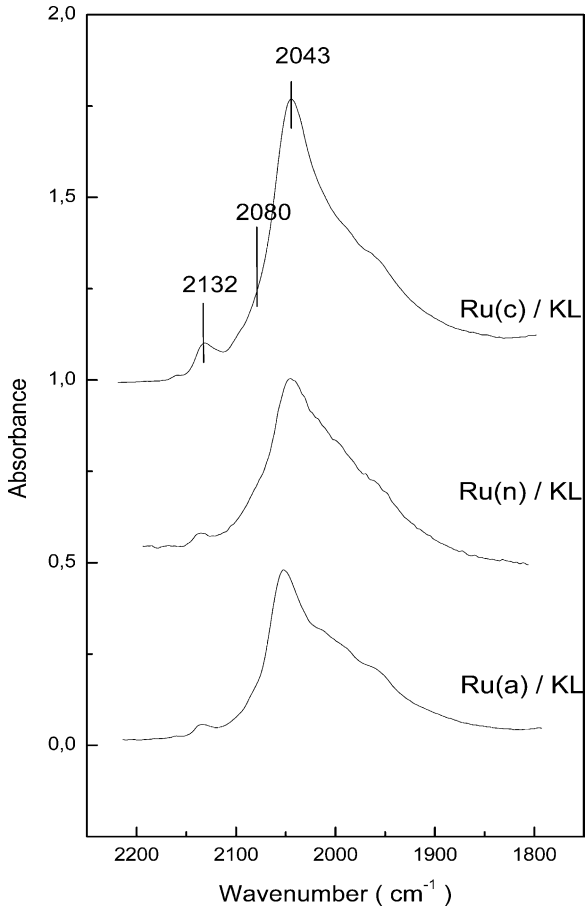

Fig. 2. FTIR spectra of CO adsorbed on the catalysts at room temperature and 2 kPa.

2100 and 1900 cm^{-1} (LF) formed by several overlapped single bands corresponding to different carbonyl-ruthenium species. Bands at wavenumbers lower than 1900 cm^{-1}, attributed to the bridged Ru-carbonyls are very weak and they were not included in Fig. 2.

Using the Fourier self deconvolution method (FSD) the wavenumber of the component bands of LF at ca. 2080, 2043, 2011, 1987, 1960 and 1920 cm^{-1} was estimated. The HF_1 band and the small shoulder at 2080 cm^{-1} (HF_2) correspond to typical multicarbonyl species associated with partially oxidized ruthenium, $Ru^{\delta+}(CO)_x$. The origin of $Ru^{\delta+}$ in reduced Ru-supported catalysts has been extensively analyzed in the literature and the results are very controversial [20–22]. In our case, since the intensity of these bands is very low, independent of their origin, a high degree of reduction of ruthenium in the catalysts is assumed.

For non-zeolitic Ru catalysts the band at 2043–2047 cm^{-1} is unambiguously assigned to CO linearly chemisorbed on non-interacting Ru^0 [20,21,23–25]. The bands at lower wavenumbers are related to different ruthenium species. Thus, for Ru/SiO_2, Kantcheva and Sayan [24] attributed a band at 1995 cm^{-1} to ruthenium with low coordination and another at 1955 cm^{-1} to bridged carbonyl species of Ru. To our knowledge, FTIR spectra of CO adsorbed on Ru/KL catalysts have not been reported, in contrast abundant studies of FTIR of CO on Pt/KL catalysts have been carried out. The published spectra show that in addition to the usual linear- and bridged-bonded CO stretching frequencies non-acidic Pt/KL catalysts display additional absorbance bands in the range of 2000–1920 cm^{-1}, which has been extensively discussed. For this type of catalysts, the overlapped bands in this range (2000–1920 cm^{-1}) have been essentially assigned to CO chemisorbed on extremely small electron rich metal particles inside the zeolite channels, with different environments [26–28], including particles with different locations and/or different degree of interaction with the framework, particles of different shape, etc. [29]. Stakheev et al [29], and Lane et al. [26], among others, attributed the electron enrichment to the interaction of platinum clusters with the walls of the zeolite channels. Menacherry and Haller [28], on other hand, proposed that the increase in electron density of the Pt particles can be caused either by a metal-support interaction or as a result of the stabilization of metal particle of specific morphology. FTIR bands at 2070–2020 cm^{-1} have also been reported for CO adsorbed on Pd/KL [26] and Ir/KL [30] and from XAFS calculations these bands were associated to small electron rich metal particles interacting with the support. Based on XAFS measurements performed on Pd/KL, Menacherry et al. [31] concluded that the morphology of the metal particles is dictated by the interaction with the zeolite lattice and claimed the formation of disc-like metal particles as a result of such interaction.

From the analysis of the spectra in Fig. 2 and the dispersion values in Table 1, we believe that an important part of the ruthenium is present in our Ru/KL catalysts as Ru^0 located at the outer surface of the zeolite (as large crystallites) not interacting with the support. The other part of the metal consist of small particles located inside of the zeolite channels in electron rich surroundings. The size of these particles must be lower than 0.7 nm, that is, the diameter of the windows of the zeolite. This partly agrees with the FTIR study by Kantcheva and Sayan [24] of CO adsorbed over Ru/SiO_2 catalysts, where they assign the 1995 cm^{-1} band to CO adsorbed on highly dispersed ruthenium. On comparing the spectra in Fig. 2, it seems that the three catalysts exhibit the same type of CO adsorbed species although the population of each one is different.

Additional information can be obtained from the FTIR spectra of the CO remaining on the catalysts after its adsorption at room temperature and subsequent evacuations at 473 K (Fig. 3). The HF bands, corresponding to CO bonded to $Ru^{\delta+}$, disappear. The LF bands decrease in intensity and the maxima are shifted to lower wavenumbers (2004–1974 cm^{-1}). According to Stakheev et al. [29], CO bonded to either electron deficient or non-interacted metal particles are easily removable, therefore the bands remaining after evacuation at 473 K can be assigned to CO bonded to the Ru particles inside the zeolite. The fact that Ru(c)/KL displays the bands at lower wavenumber (1974 cm^{-1}) confirms that, in this sample, ruthenium inside of the zeolite is more electron rich than in the other catalysts. It is important to point out that the band at ca. 1974 cm^{-1} has been also reported for Pt/KL, Pd/KL and Ir/KL catalysts and related to small particles of metal strongly interacting with the walls of the zeolite.

Fig. 4 shows the differential heats of CO adsorption (Q_{ads}) at 330 K as a function of surface coverage for Ru(c)/KL, Ru(n)/KL and Ru(a)/KL samples. The extent of carbon monoxide coverage, θ, for a sample was determined by the ratio of the adsorbed amount at a given point and the amount necessary to form the monolayer. This procedure facilitates the comparative study of catalysts with different dispersions. The Ru(c)/KL sample exhibits an initial heat of adsorption of 150 kJ/mol, which subsequently decreases to a large plateau at ca. 120 kJ/mol, in the region of $\theta = 0.10$–0.8. The higher initial adsorption heats obtained on this sample can be ascribed to CO strongly bonded to surface the Ru atoms probably located inside the zeolite cavities, in agreement with the FTIR spectrum of this catalyst (Fig. 3). The heat of adsorption observed in the plateau is usually assigned to linearly adsorbed CO on different ruthenium sites in Ru/C and Ru/Al_2O_3 [32], Ru/SiO2 [33] Ru polycrystalline and Ru/TiO_2 [34]. At high coverage ($\theta = 0.85$–0.95), this sample exhibits a small plateau at 95 kJ/mol associated to $Ru^{\delta+}(CO)_2$ species [35]. The Ru(n)/KL sample exhibits an initial heat of adsorption of 128 kJ/mol which also decreases

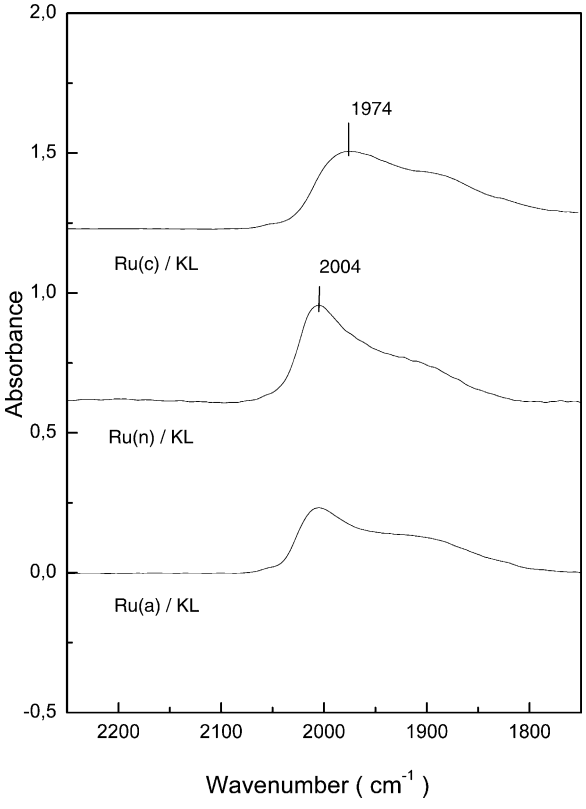

Fig. 3. FTIR spectra of the CO remaining on the catalysts upon adsorption at room temperature and subsequent evacuation at 473 K and 10^{-2} Pa.

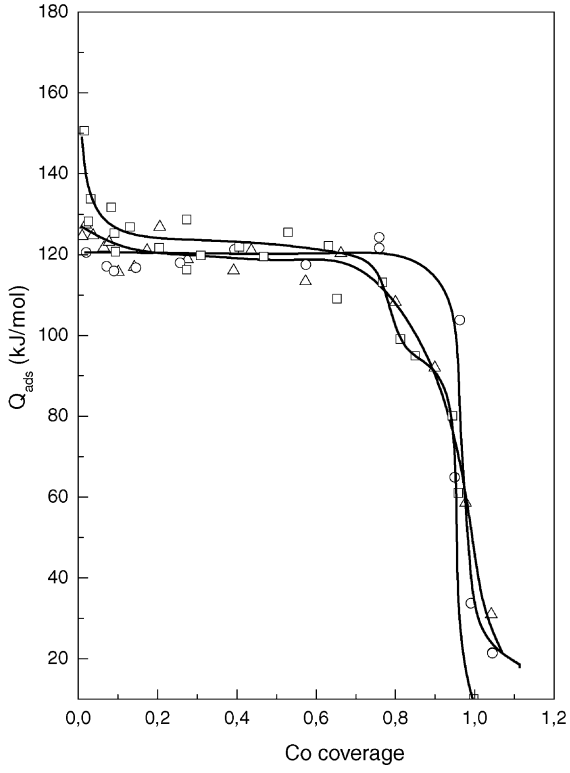

Fig. 4. Differential heats of CO chemisorption at 330 K as a function of surface coverage for the different catalysts: (○) Ru(a)/KL, (△) Ru(n)/KL and (□) Ru(c)/KL.

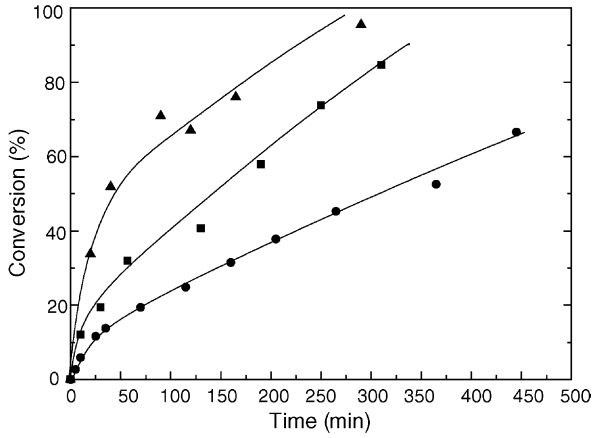

Fig. 5. Temporal citral conversion profiles for citral hydrogenation over: (●) Ru(a)/KL, (▲) Ru(n)/KL and (■) Ru(c)/KL.

to a large plateau at ca. 120 KJ/mol, in the region of $\theta = 0.10$–0.8. In contrast, Ru(a)/KL exhibits an uniform heat of adsorption of 120 kJ/mol for the whole range of coverage. Thus, the three catalysts show a large range of energetically homogenous surface sites and only differ in the region of the initial heat of adsorption. We also found that there is a relationship between CO adsorption heat values and the average metal particle sizes of the catalysts, i.e. electronic and active site location effects are present in our case. This is in agreement with the information deduced from the species detected by CO-FTIR for this sample. Probably, the electronic factors should be related with the surface Ru sites on the small particles located in the channels of the KL-zeolite. Moreover, comparing our calorimetric results with those in the literature [36,37] for CO adsorption over different Ru crystallographic planes (105–120 kJ/mol) we can suggest that the Ru nanoparticles present in our catalysts are mainly exposing (1 0 0) and (1 1 0) faces.

Table 2
Catalytic properties in the hydrogenation of citral over the KL-zeolite ruthenium catalysts

Catalyst	a_0 (μmol g^{-1} s^{-1})	TOF (s^{-1})
Ru(c)/KL	1.55	0.017
Ru(n)/KL	1.03	0.017
Ru(a)/KL	0.67	0.019

a_0, initial hydrogenation activity of the catalysts; TOF, initial turn-over number.

3.2. Catalytic activity measurements

Activity of the catalysts was evaluated in the hydrogenation of citral (isomers E + Z) in the liquid phase using 2-propanol as solvent. Fig. 5 shows the conversion of citral as a function of the reaction time for the three catalysts. From the initial slope of the curves, the initial activity (a_0) and the corresponding turn-over frequency (TOF) have been calculated for each catalyst. These values are displayed in Table 2. In spite of the initial activity differences, which vary in the order: Ru(c)/KL > Ru(n)/KL > Ru(a)/KL, the TOFs of the three catalysts are similar (close to 0.020 s^{-1}), indicating that hydrogenation of citral is a structure-insensitive reaction. This finding is in agreement with those reported by other authors [38] who evaluated Ru-supported

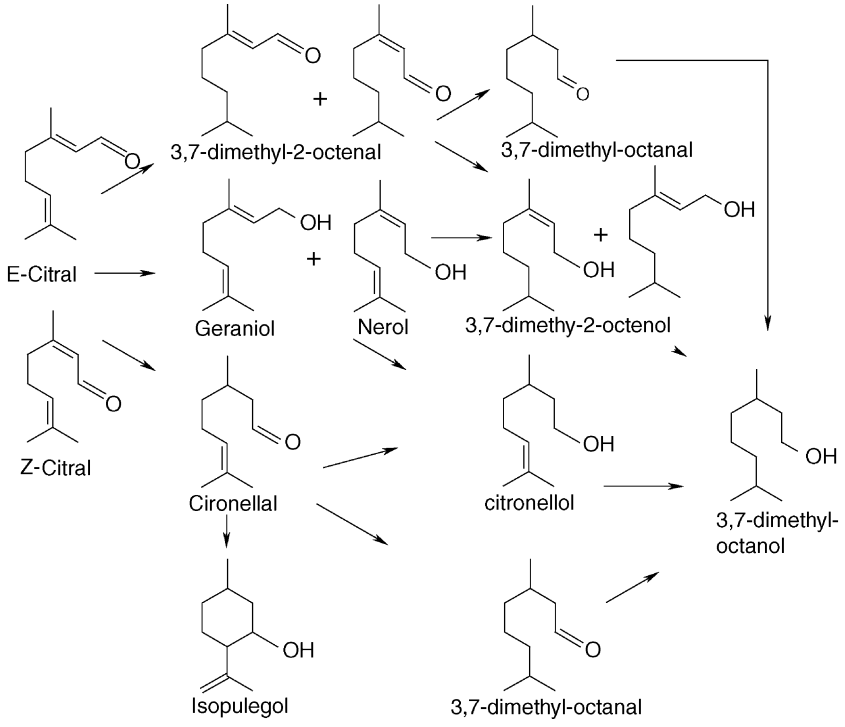

Scheme 1.

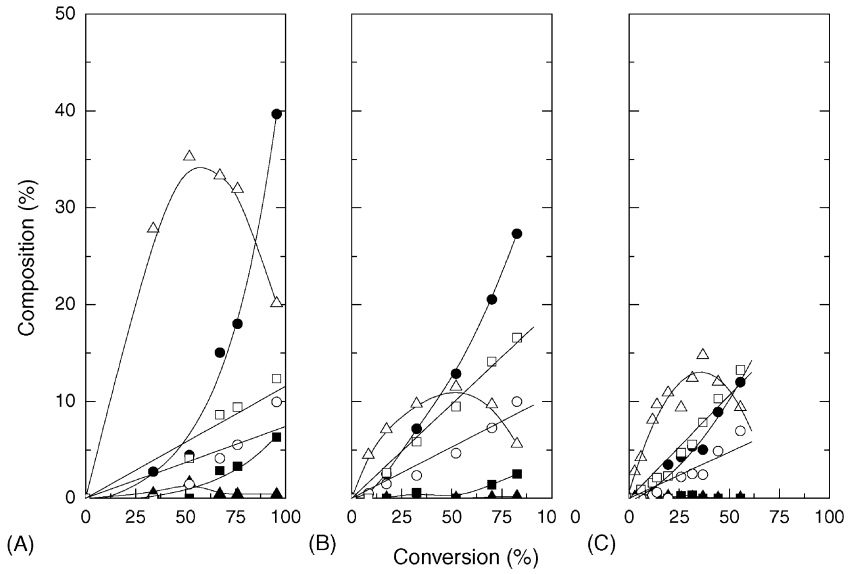

Fig. 6. Products distribution as a function of citral conversions. Ru(c)/KL (A), Ru(n)/KL (B) and Ru(a)/KL (C). *Symbols*: (△) citronellal, (○) nerol, (□) geraniol, (▲) isopulegol, (●) citronellol and (■) 3,7-dimethyloctanol.

catalysts in the same reaction. On other hand, in all the cases citronellal, geraniol and nerol were obtained as partial hydrogenation products, together with citronellol and dimethyloctanol as a result of the subsequent hydrogenation reactions. A small amount of isopulegol, produced by cyclization of citronellal, was also obtained while acetals were never detected. These results agree with the non-acidic character of the KL zeolite, since both reactions, cyclization and acetylation occur on acid sites [39]. The routes of formation of all products from citral hydrogenation are given in Scheme 1. Plots in Fig. 6 show the product composition as a function of citral conversion for Ru(c)/KL, Ru(n)/KL and Ru(a)/KL. For the three catalysts, the concentration of citronellal increases from the beginning of reaction, it passes through a maximum and then declines at conversions higher than 40–50%, probably due to its transformation to citronellol (Scheme 1), this latter increases through the conversion range. Unsaturated alcohols, geraniol and nerol, appear from the beginning of reaction and their formation increases continuously. When comparing the product distribution for the three catalysts at the same conversion level, it is observed that concentration of citronellal follows the trend: Ru(c)/KL > Ru(n)/KL > Ru(a)/KL, while that of geraniol + nerol is in the opposite order. This indicates an evident effect on the selectivity induced by the ruthenium precursors used in the catalysts preparation. Thus, at conversion level close to 50%, when the concentration maximum of citronellal was reached, the percentage of this compound in the product is 36% for Ru(c)/KL, 12% for Ru(n)/KL and 10% for Ru(a)KL.

The differences of selectivity observed can be tentatively explained from the characterization results. From data in Table 1, it can be observed that the lower the average crystal size (2.8 nm) the higher the formation of citronellal, while the higher selectivity toward geraniol + nerol is achieved for ruthenium catalysts with higher particle sizes 4.5–7.3 nm. It is important to point out, that from FTIR and microcalorimetry results we have found evidences that part of ruthenium particles are located inside the zeolite as small electron enriched particles, being their population the maximum in the Ru(c)/KL sample. The fact that this catalyst exhibits the highest selectivity to citronellal suggests that these ruthenium particles are particularly appropriated to activate and hydrogenate the C=C bond. It is probable that the nature of the metal precursor and the solvents used in the catalysts preparation govern the metal-support interaction and, consequently, the size, the shape, the distribution, the electronic state and, even, the location of the Ru particles in the zeolite.

4. Conclusions

Catalysts prepared by impregnation of KL-zeolite with different precursors, and after reduction at 673 K, have been characterized and studied in the hydrogenation of citral at 323 K of constant temperature and 5 MPa of hydrogen pressure. The main reaction products were citronellal, nerol, geraniol and citronellol. Hydrogenation activity correlates to the metal dispersion, whereas the TOF is independent on the metal dispersion and consequently does not depend on the used ruthenium precursor employed. The selectivity towards unsaturated alcohols, geraniol and nerol, follows the order Ru(c)/KL < Ru(n)/KL < Ru(a)/KL, while the selectivity toward citronellal is in the opposite order. Small ruthenium particles (2.8 nm in catalyst Ru(c)/KL) seem to be in interaction with the walls of the zeolite, and this induces a maximum of citronellal selectivity in the reaction. In contrast, larger ruthenium particles, which are present in Ru(n)/KL and Ru(a)/KL samples favor the formation of unsaturated alcohols in the detriment of citronellal.

Acknowledgement

The financial support of the MEC of Spain under Projects MAT2002-04189-C02-01 and 02 is acknowledged.

References

[1] P. Gallezot, D. Richard, Cat. Rev.—Sci. Eng. 40 (1998) 81.
[2] F. Delbecq, P. Sautet, J. Catal. 152 (1995) 217.
[3] U.K. Singh, M.A. Vannice, J. Catal. 199 (2001) 73.
[4] P. Gallezot, A. Giroir-Fendler, D. Richard, Catal. Lett. 4 (1990) 169.
[5] P. Gallezot, B. Blanc, D. Barthomeuf, M.I. Païs da Silva, Stud. Surf. Sci. Catal. 84 (1994) 1433.
[6] D. Tas, R.F. Parton, K. Vercruysse, P. Jacobs, Stud. Surf. Sci. Catal. 105 (1997) 1261.
[7] P. Mäki-Arvela, L.P. Tiainen, A.K. Neyestanaki, R. Sjöholm, R.K. Rantakylä, E. Laine, T. Salmi, D.Y. Murzin, Appl. Catal. A. 237 (2002) 181.
[8] D.W. Breck, Zeolite Molecular Sieves. Structure, Chemistry and Use, Wiley & Sons, New York, 1974, p. 113.
[9] W. Han, A.B. Kooh, R.F. Hicks, Catal. Lett. 18 (1993) 219.
[10] E. Iglesia, J.E. Baumgartner, Stud. Surf. Sci. Catal. 75 (1993) 993.
[11] P.V. Menacherry, G.L. Haller, J. Catal. 177 (1998) 175.
[12] K. Lu, B.J. Tatarchuk, J. Catal. 106 (1987) 166.
[13] E. Miyazaki, J. Catal. 65 (1980) 84.
[14] B. Bachiller-Baeza, I. Rodríguez-Ramos, A. Guerrero-Ruiz, Langmuir 14 (1998) 3556.
[15] T. Narita, H. Miura, K. Sugiyama, T. Matsuda, J. Catal. 103 (1987) 491.
[16] J.R. Anderson, Structure of Metallic Catalysts, Academic Press, New York, 1975, p. 295.
[17] B. Bachiller-Baeza, A. Guerrero-Ruiz, P. Wang, I. Rodríguez-Ramos, J. Catal. 204 (2001) 450.
[18] G. Neri, L. Mercadante, A. Donato, A.M. Visco, S. Galvagno, Catal. Lettt. 29 (1994) 379.
[19] S. Galvagno, C. Milone, Catal. Lettt. 18 (1993) 349.
[20] K. Hadjiivanov, J.C. Lavalley, J. Lamotte, F. Maugé, J. Saint-Just, M. Che, J. Catal. 176 (1998) 415.
[21] G.H. Yokomizo, C. Louis, A.T. Bell, J. Catal. 120 (1989) 1.
[22] J.A. de los Reyes, M. Vrinat, M. Breysse, F. Mauge, J. LaValley, Catal. Lett. 13 (1992) 213.
[23] J.M. Grau, X.L. Seoane, A. Arcoya, Catal. Lett. 83 (2002) 247.
[24] M. Kantcheva, S. Sayan, Catal. Lett. 60 (1999) 27.
[25] C. Elmasides, C.I. Kondarides, S.G. Neophytides, X.E. Verykios, Stud. Surf. Sci. Catal. 130 (2000) 3083.
[26] G.S. Lane, J.T. Miller, F.S. Modica, M.K. Barr, J. Catal. 141 (1993) 465.
[27] W.H. Han, A.B. Kooh, R.F. Hicks, Catal. Lett. 18 (1993) 193.
[28] P.V. Menacherry, G.L. Haller, J. Catal. 177 (1998) 175.
[29] A.Y. Stakheev, E.S. Shpiro, E.I. Jaeger, G.S. Schulz-Ekloff, Catal. Lett. 32 (1995) 147.
[30] N.D. Triantafillou, S.E. Deutsh, O. Alexeev, J.T. Miller, B.C. Gates, J. Catal. 159 (1996) 14.
[31] P. Menacherry, M. Fernández, G.L. Haller, J. Catal. 166 (1997) 75.
[32] A. Guerrero-Ruiz, A. Maroto-Valiente, M. Cerro-Alarcón, B. Bachiller-Baeza, I. Rodríguez-Ramos, Top. Catal. 19 (2002) 303.
[33] J.M. Hill, R. Alcala, R.M. Watwe, J. Shen, J.A. Dumesic, Catal. Lett. 68 (2000) 129.
[34] V.P. Londhe, N.M. Gupta, J. Catal. 169 (1997) 415.
[35] O. Dulaurent, K. Chandes, C. Bouly, D. Bianchi, J. Catal. 192 (2000) 262.
[36] B.E. Koel, G.A. Somorjai, in: J.R. Anderson, M. Boudart (Eds.), Catalysis: Science and Technology, vol. 7, Springer-Verlag, Berlin, 1985, Chapter 3, p. 211.
[37] T.E. Madey, D. Menzel, in: H. Kumagai, T. Toya (Eds.), Proceedings of the second International Conference on Solid Surface, 1974, p. 229.
[38] L. Mercadante, G. Neri, C. Milone, A. Donato, S. Galvagno, J. Mol. Catal. A 105 (1996) 93.
[39] C. Milone, C. Gangemi, R. Ingoglia, G. Neri, S. Galvagno, Appl. Catal. A 184 (1999) 89.